

Electronic Supplementary Information

Disc-like 7, 14-Dicyano-ovalene-3,4:10,11-bis(dicarboximide) as a Solution-Processible n-Type Semiconductor for Air Stable Field-Effect Transistors

Jinling Li,^{a,‡} Jing-Jing Chang,^{a,‡} Huei Shuan Tan,^b Hui Jiang,^c Xiaodong Chen,^c Zhikuan Chen,^b Jie Zhang^b and Jishan Wu^{*a,b}

^a Department of chemistry, National University of Singapore, 3 Science Drive 3, 117543, Singapore. Fax: 65 6779 1691; Tel: 65 6516 2677; E-mail: chmwuj@nus.edu.sg

^b Institute of Materials Research and Engineering, A*Star, 3 Research Link, 117602, Singapore.

^c School of Materials Science and Engineering, Nanyang Technological University, 50 Nanyang Avenue, 639798, Singapore

‡ These authors contributed equally to this work.

1. General experimental method

All reagents and starting materials were obtained from commercial suppliers and used without further purification. Tetrahydrofuran (THF) was purified by routine procedure and distilled over sodium under nitrogen before using. Bisanthenequinone was prepared according to literature (S. M. Arabei, T. A. Pavich, *J. Appl. Spectr.* **2000**, 67, 236). 2-Decyltetradecan-1-amine was prepared according to previous report (X. W. Zhan et al. *J. Am. Chem. Soc.* **2007**, 129, 7246). Column chromatography was performed on silica gel 60 (Merck 40-60 nm, 230-400 mesh). All NMR spectra were recorded on the Bruker AMX500 spectrometer. All chemical shifts are quoted in ppm, relative to tetramethylsilane, using the residual solvent peak as a reference standard. MALDI-TOF MS spectra were measured on a Bruker Autoflex MALDI-TOF instrument, using 1,8,9-trihydroxyanthracene as a matrix. UV-vis absorption was recorded on Shimadzu UV-1700 spectrometer. The solvents used for UV-vis and PL measurements are of HPLC grade (Merck). The electrochemical measurements were carried out in anhydrous chlorobenzene with 0.1 M tetrabutylammonium hexafluorophosphate (Bu₄NPF₆) as the supporting electrolyte at a scan rate of 0.05 V/s at room temperature under the protection of nitrogen. A gold disk was used as working electrode, platinum wire was used as counter electrode, and Ag/AgCl (3M KCl solution) was used as reference electrode. The potential was externally calibrated by using ferrocene as reference. Thermogravimetric analysis (TGA) was carried out on a TA instrument 2960 at a heating rate of 10 °C/min under

nitrogen flow. Differential scanning calorimetry (DSC) was performed on a TA instrument 2920 at a heating /cooling rate of 10 °C/min under nitrogen flow. Polarizing optical microscope (POM) measurements were conducted on the OLYMPUS BX51 equipped with the Linkam TP94 programmable hot stage. X-ray diffraction (XRD) patterns of the thin film and powder were measured on a Bruker-AXS D8 DISCOVER with GADDS X-ray diffractometer. Copper K α line was used as a radiation source with $\lambda = 1.5406 \text{ \AA}$. Tapping-mode AFM was performed on a Nanoscope V microscope (Veeco Inc.).

2. Synthetic procedures and characterization data

N,N'-bis(2-decyltetradecyl)-ovalene-3,4:10,11-bis(dicarboxylic anhydride) (**3**): Four portion of zinc powder (4 x 6 g) and 80% acetic acid (4 x 10 mL) were added in 30-minute intervals to a refluxing suspension of bisanthenequinone in pyridine (200 mL). The yellow suspension became green, then brown. After 5 h, the solution was cooled to room temperature, the zinc powder filtered off, and water (1 L) added. The precipitate thus formed was filtered off and dried under vacuum to yield 1.6 g of a yellow insoluble solid. This solid was heated at reflux for 12 h with maleic anhydride (5 g) in nitrobenzene (60 mL). A color change from greenish yellow via blue and violet to brown was observed during warming and the first 30 minutes at reflux. Chloroform was added to the cooled solution, and the insoluble solid was filtered off, washed with chloroform, and dried under vacuum to yield crude dianhydride **3** as an insoluble material.

N,N'-bis(2-decyltetradecyl)-ovalene-3,4:10,11-bis(dicarboximide) (**ODI**): Crude dianhydride **3** (1 g, 1.86 mmol), 2-decyltetradecan-1-amine (3.28 g, 9.28 mmol), and 200 mL of DMF were heated under nitrogen at 175 °C overnight. The reaction mixture was cooled to room temperature and 200 mL of methanol was added. The red solid was collected by vacuum filtration and washed with methanol for several times, dried under vacuum, and then further purified by column chromatography on silica gel with DCM: Hexane = 1:1 (v/v) as eluent to afford **ODI** (1.84 g, 82%) as deep red solid. ¹H NMR (500 MHz, Cl₂CDCDCl₂, 100 °C), δ ppm = 0.96 (m, 12H, -CH₃), 1.34-1.74 (m, 80H, -CH₂), 2.31 (br, 2H, -CH), 4.01 (d, $J = 6.9$ Hz, 4H, -CH₂), 7.60 (d, $J = 8.2$ Hz, 4 H, Ar), 7.65 (s, 2 H Ar), 8.73 (d, $J = 8.2$ Hz, 4 H Ar). ¹³C NMR (125 MHz, Cl₂CDCDCl₂, 100 °C), δ ppm = 13.52, 13.55, 22.21, 22.25, 26.49, 28.94, 29.00, 29.32, 29.40, 29.45, 29.48, 29.99, 31.55, 31.60, 32.07, 37.60, 42.68, 114.91, 115.00, 119.48, 121.09, 121.74, 121.79, 123.14, 126.03, 127.63, 168.99. MS (MALDI-TOF): $m/z = 1209.51$; High resolution (HR) MS (MALDI-TOF): $m/z = 1208.8250$, calculated for C₈₄H₁₀₈N₂O₄: 1208.8304 (error = -4.44 ppm).

7,14-Dibromo-N,N'-bis(2-decyltetradecyl)-ovalene-3,4:10,11-bis(dicarboximide) (**ODI-Br**): **ODI** (500 mg, 0.41 mmol), bromine (0.1 mL) in 100 mL of CHCl₃ was reacted at room temperature for 5 days. The organic layer was extracted with CHCl₃ and washed with Na₂SO₃ aqueous solution for several times. The organic layer was concentrated and further purified by column chromatography on silica gel with CDCl₃: Hexane = 1:2 (v/v) as eluent to afford **ODI-Br** as deep red solid in 85% yield. ¹H NMR (500 MHz, Cl₂CDCDCl₂, 100 °C), δ ppm = 0.99 (m, 12H, -CH₃), 1.34-1.62 (m, 80H, -CH₂), 2.17 (br, 2H, -CH), 3.82 (br, 4H, -CH₂), 7.35 (br, 4 H, Ar), 8.21 (br, 4 H, Ar). ¹³C NMR (125 MHz, Cl₂CDCDCl₂, 100 °C), δ ppm = 13.61, 13.63, 22.29, 22.32, 26.31, 29.01, 29.06, 29.29, 29.39, 29.46, 29.49, 29.99, 31.62, 31.66, 31.86, 37.45, 42.57, 113.19, 116.75, 119.78, 120.77, 121.67, 122.22, 123.15, 126.35, 167.87. MS (MALDI-TOF): m/z = 1367.24; HR MS (MALDI-TOF): m/z = 1364.6447, calculated for C₈₄H₁₀₆Br₂N₂O₄: 1364.6514 (error = -4.90 ppm).

7,14-Dicyano-N,N'-bis(2-decyltetradecyl)-ovalene-3,4:10,11-bis(dicarboximide) (**ODI-CN**): **ODI-Br** (100 mg, 0.07 mmol), copper cyanide (65 mg, 0.73 mmol), 1,1'-bis(diphenylphosphino)-ferrocene (12.7 mg, 0.02 mmol), tris(dibenzylideneacetone)-dipalladium (5.4 mg, 0.01 mmol) were combined in dry *p*-dioxane (20 mL) and refluxed for 2 days under nitrogen atmosphere. The crude product was filtered through glass funnel, and washed with methanol, and then further purified by column chromatography on silica gel with hot CHCl₃ as eluent to afford **ODI-CN** (78 mg, 86%) as red solid. ¹H NMR (500 MHz, Cl₂CDCDCl₂, 100 °C), δ ppm = 0.92 (m, 12H, -CH₃), 1.33-1.73 (m, 80H, -CH₂), 2.37 (br, 2H, -CH), 4.18 (d, *J* = 6.3 Hz, 4H, -CH₂), 8.34 (d, *J* = 8.85 Hz, 4H, Ar), 9.33 (d, *J* = 8.85 Hz, 4H, Ar). ¹³C NMR (125 MHz, Cl₂CDCDCl₂, 100 °C), δ ppm = 13.52, 13.55, 22.21, 22.25, 26.40, 26.42, 28.93, 28.99, 29.31, 29.37, 29.38, 29.43, 29.92, 31.54, 31.59, 32.00, 37.62, 43.37, 105.10, 114.08, 114.83, 116.45, 118.61, 121.44, 124.29, 125.32, 125.40, 127.17, 167.85. MS (MALDI-TOF): m/z = 1259.18; HR MS (MALDI-TOF): m/z = 1258.8221, calculated for C₈₆H₁₀₈N₄O₄: 1258.8209 (error = 0.98 ppm).

3. Photophysical and electrochemical properties of ODI and ODI-CN

The UV-vis absorption and fluorescence spectra of ODI and ODI-CN are shown in Figures S1. The cyclic voltammograms of ODI and ODI-CN are shown in Figure S2. The data are collected in Table S1.

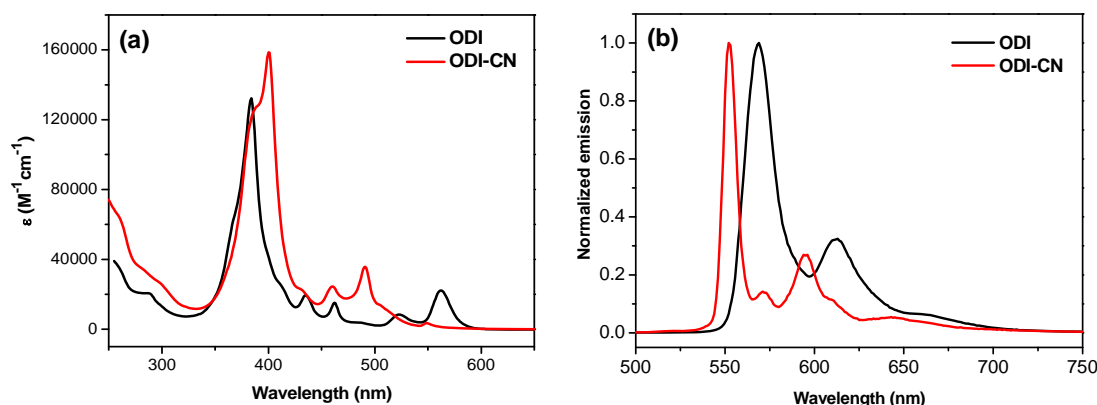


Figure S1. (a) UV-vis absorption spectra in dilute chloroform solutions (concentration = 1×10^{-5} M); (b) fluorescence spectra of ODI and ODI-CN in dilute chloroform solutions (concentration = 1×10^{-6} M, excitation wavelength was 521 nm and 491 nm for ODI and ODI-CN, respectively).

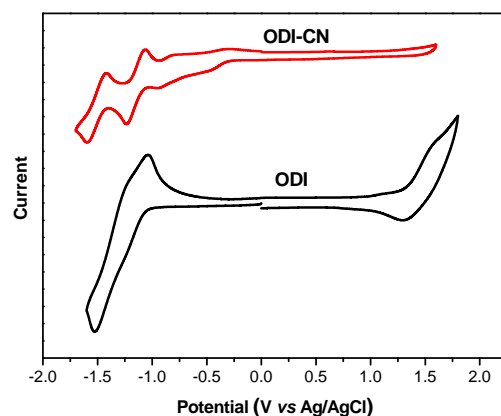


Figure S2. Cyclic voltammograms of ODI and ODI-CN in chlorobenzene with 0.1 M Bu_4NPF_6 as the supporting electrolyte.

Table S1. Summary of photophysical and electrochemical properties of ODI and ODI-CN.

Compound	λ_{abs} (nm)	λ_{em} (nm)	E_{ox}^1 (V)	E_{red}^1 (V)	E_{red}^2 (V)	E_{red}^3 (V)	E_{red}^4 (V)	HOMO (eV)	LUMO (eV)	E_g^{opt} (eV)
ODI	560, 521, 462, 435	384, 568, 612	1.1	-1.17	-1.40	-	-	-5.54	-3.14	2.14
ODI-CN	548, 491, 460, 431	401, 552, 595	-	-0.43	-0.85	-1.14	-1.51	-6.13	-3.90	2.23

E_{ox}^n and E_{red}^n are half-wave potentials for respective redox waves with AgCl/Ag as reference. HOMO and LUMO energy levels were calculated from the onset potentials of the first oxidation ($E_{\text{ox}}^{\text{onset}}$) and the first reduction wave ($E_{\text{red}}^{\text{onset}}$) according to the following equations: $\text{HOMO} = -(4.8 + E_{\text{ox}}^{\text{onset}})$ and $\text{LUMO} = -(4.8 + E_{\text{red}}^{\text{onset}})$, where the potentials are referred to $E_{\text{Fc}^+/\text{Fc}}$ with ferrocene as external reference. The HOMO level of **ODI-CN** was calculated from the optical energy gap (E_g^{opt}).

4. Variable-temperature ^1H NMR (500 MHz) spectra of ODI-CN

Both ODI and ODI-CN have strong tendency to aggregate in solution as revealed by variable-temperature ^1H NMR measurements. In particular, ^1H NMR spectrum of **ODI-CN** only shows broad resonances in the aromatic region at room temperature and the peaks are gradually shifted to low field and become well-split upon heating to higher temperatures (Figure S3). This is a good sign that **ODI-CN** molecules have strong intermolecular association *via* π - π interactions in solution. However, determination of the associate constant at room temperature by measuring the ^1H NMR spectra of solutions with different concentrations is not feasible because of the poor solubility of ODI-CN at RT.

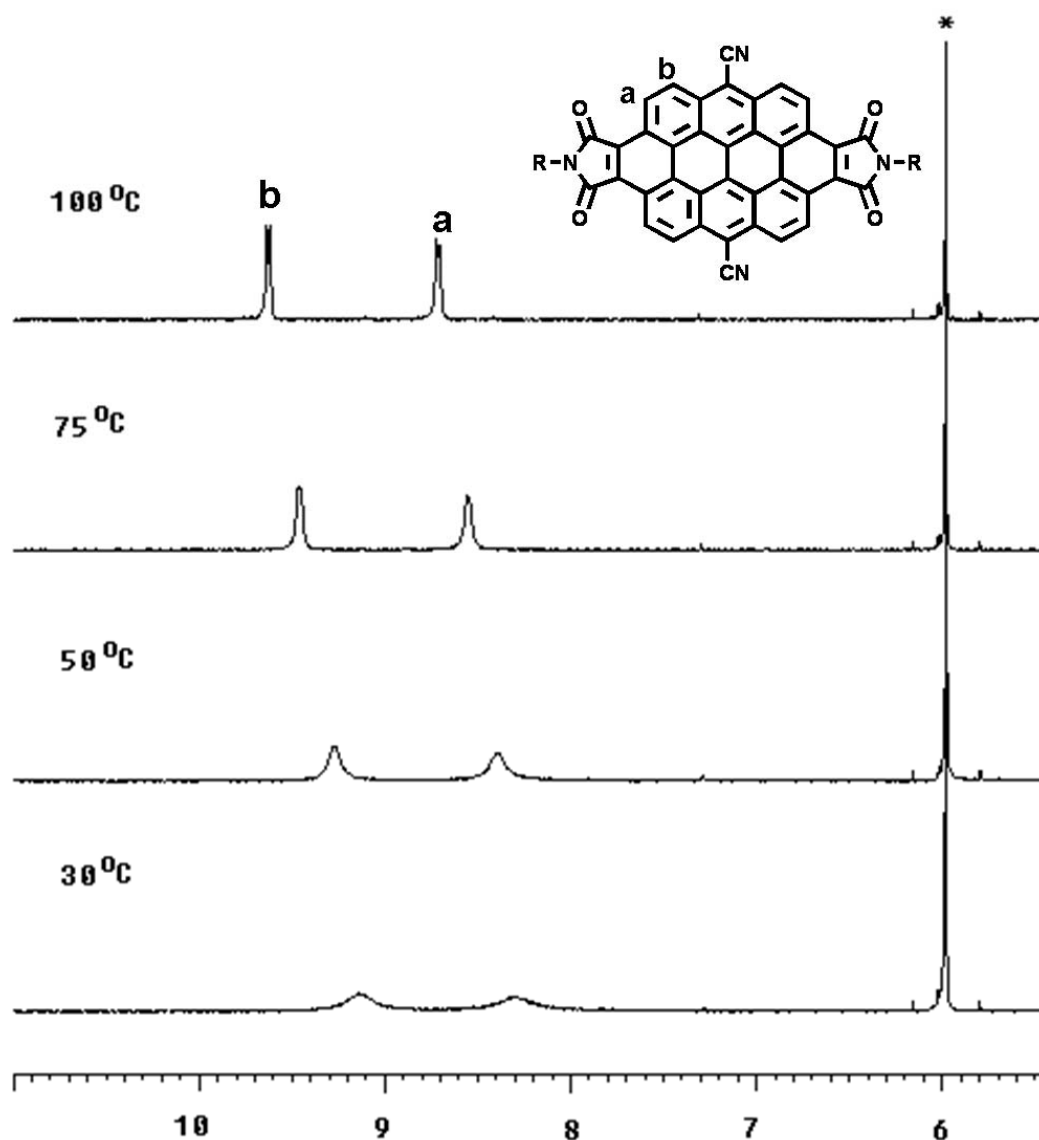


Figure S3. Variable-temperature ^1H NMR (500 MHz) spectra (aromatic region) of ODI-CN in $[\text{D}_2]$ tetrachloroethane.

5. Thermogravimetric analysis (TGA) curves

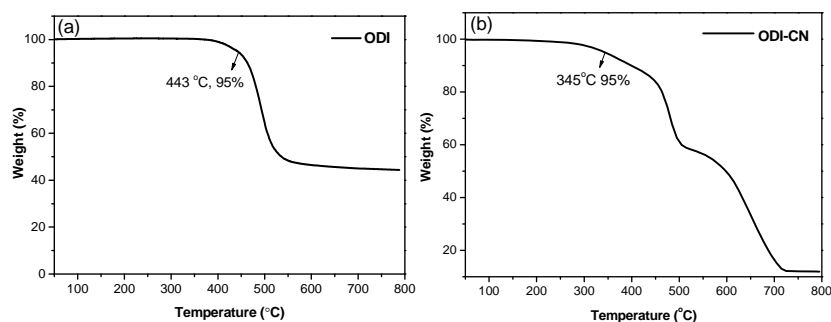


Figure S4. Thermogravimetric analysis (TGA) curves of ODI (a) ODI-CN (b).

6. Differential scanning calorimetry (DSC) thermograms

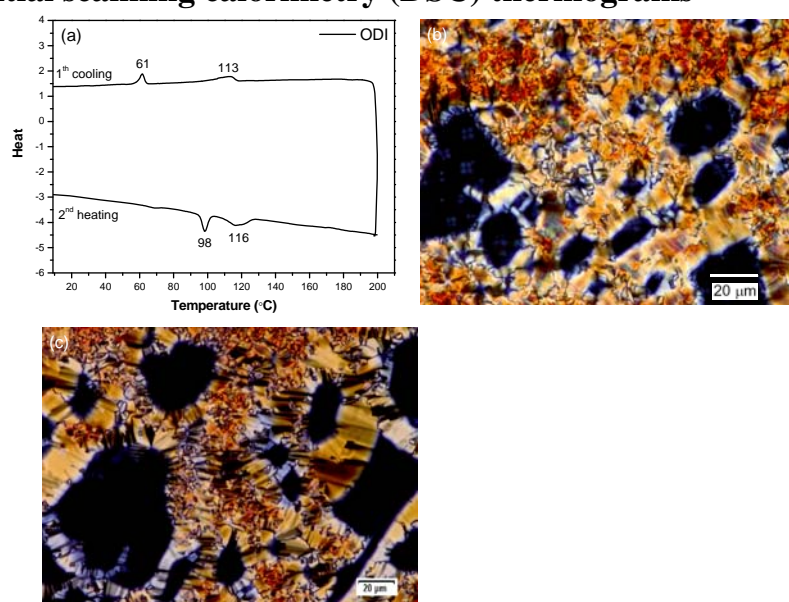


Figure S5. Differential scanning calorimetry (DSC) thermograms of ODI (second heating and first cooling scans are given, 10 °C min⁻¹ under N₂, (a)) and polarizing optical microscopy (POM) image of ODI at 100 °C during cooling (b) and at 350 °C during heating (c).

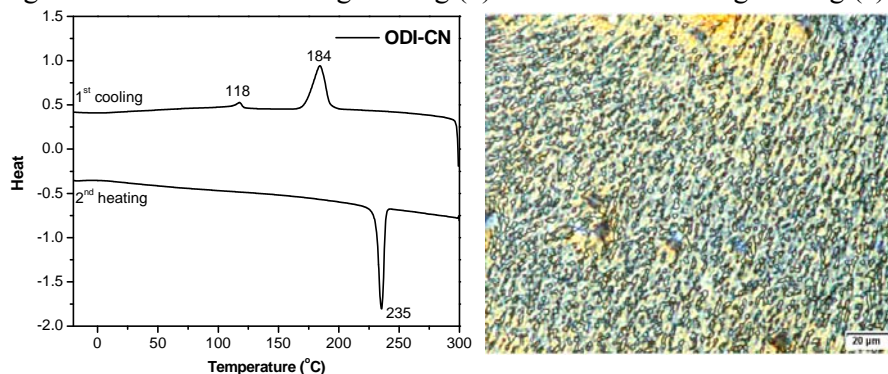


Figure S6. Differential scanning calorimetry (DSC) thermograms of ODI-CN (second heating and first cooling scans are given, 10 °C min⁻¹ under N₂, left) and polarizing optical microscopy image of ODI-CN at 300 °C during heating.

7. Powder X-ray diffraction (XRD) patterns

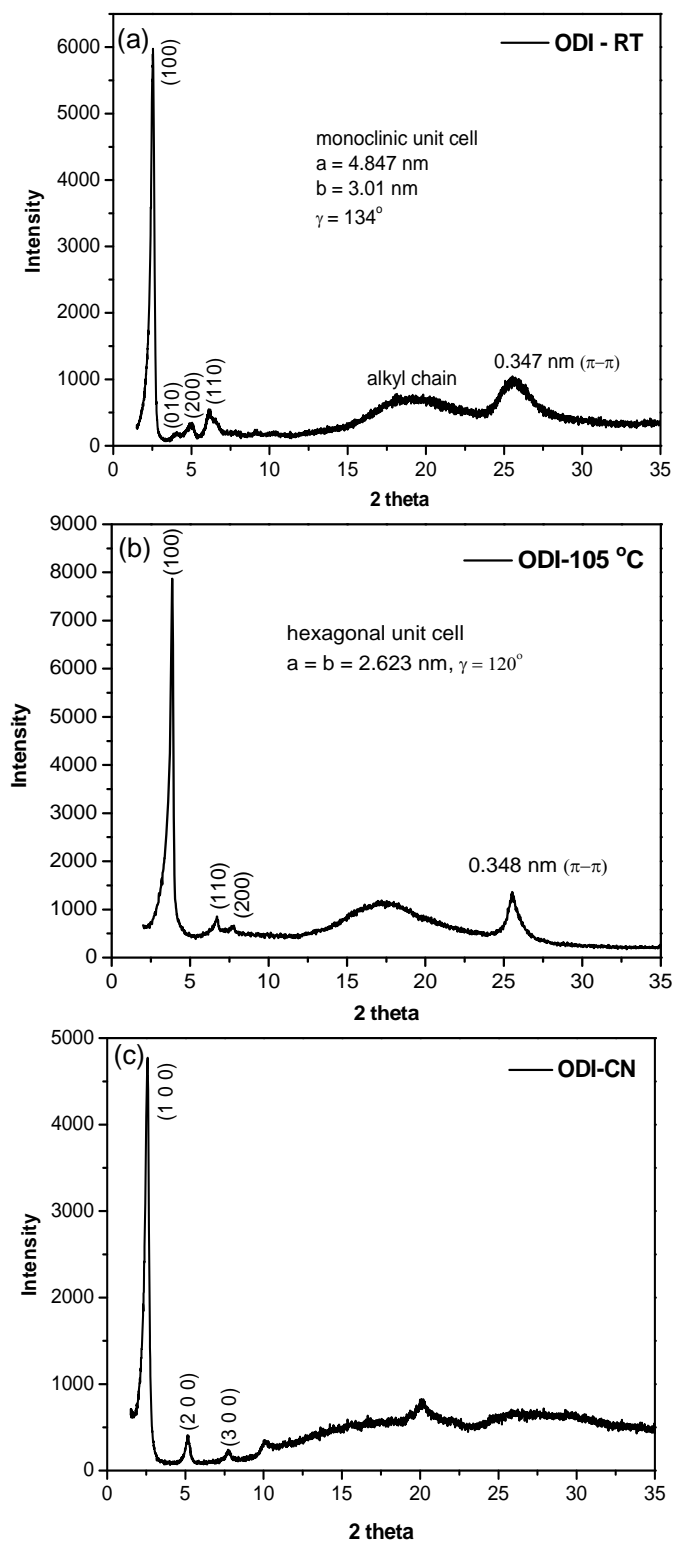


Figure S7. Powder X-ray diffraction (XRD) patterns of (a) ODI at room temperature; (b) ODI at 105 °C and (c) ODI-CN at room temperature. XRD pattern of ODI measured at 140 °C is very similar to that measured at 105 °C (b), indicating a very similar liquid crystalline phase.

8. FET characteristics of ODI-CN

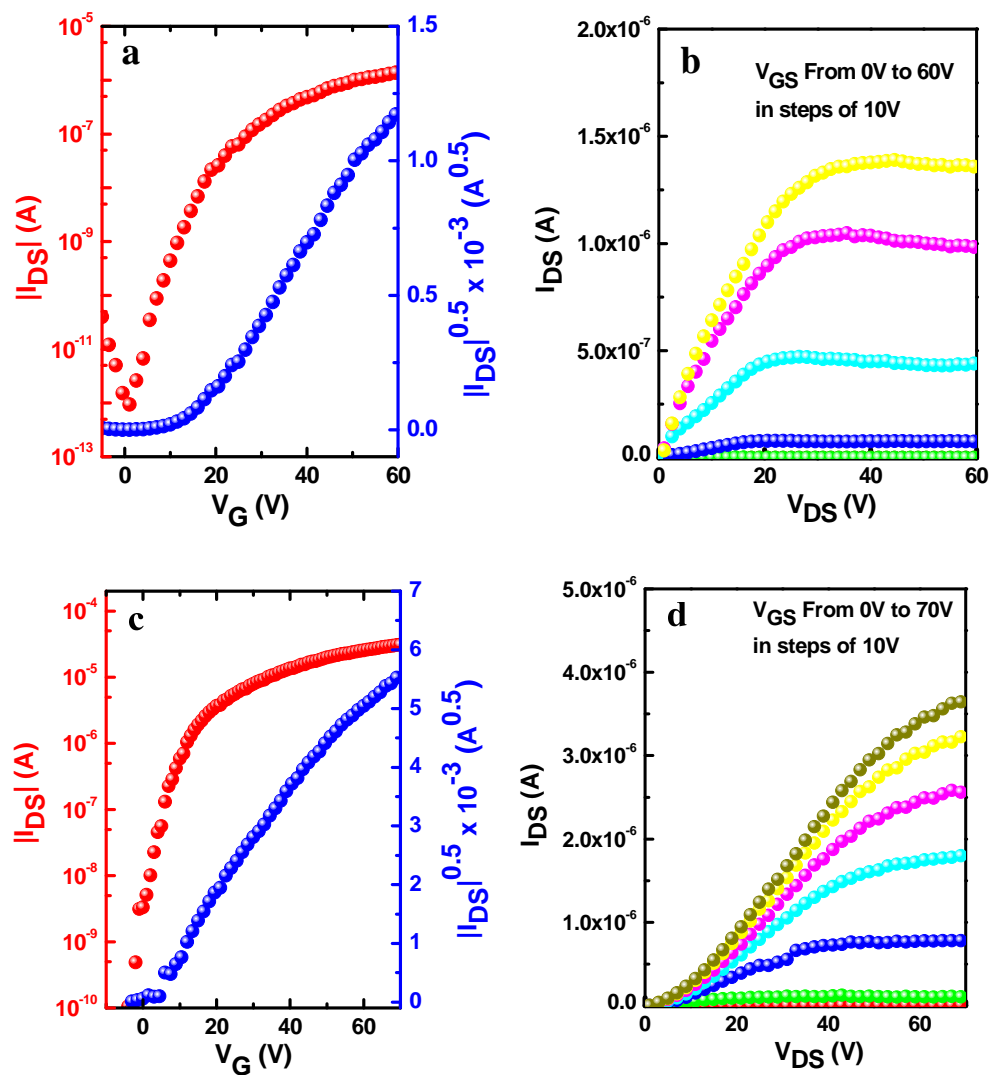


Figure S8. Transfer (a, c) and output (b, d) characteristic of the OFETs based on ODI-CN. The thin film was prepared from DCB solution on OTCS treated SiO₂/Si substrate followed by annealing at 230 °C. The devices were measured in air (a, b) and nitrogen (c, d).

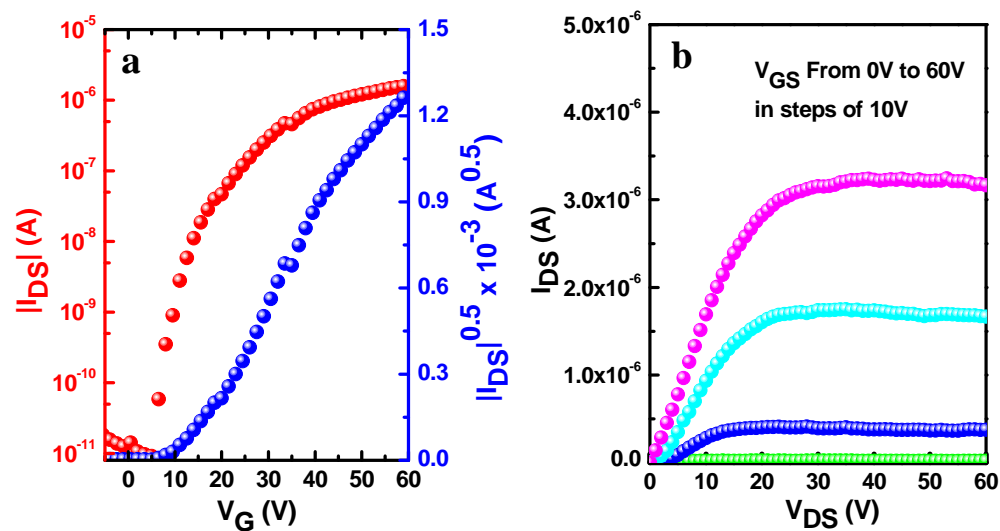


Figure S9. Transfer (a) and output (b) characteristic of the OFETs based on ODI-CN. The thin film was prepared from CHCl_3 solution on OTCS treated SiO_2/Si substrate followed by annealing at 230°C . The devices were measured in air.

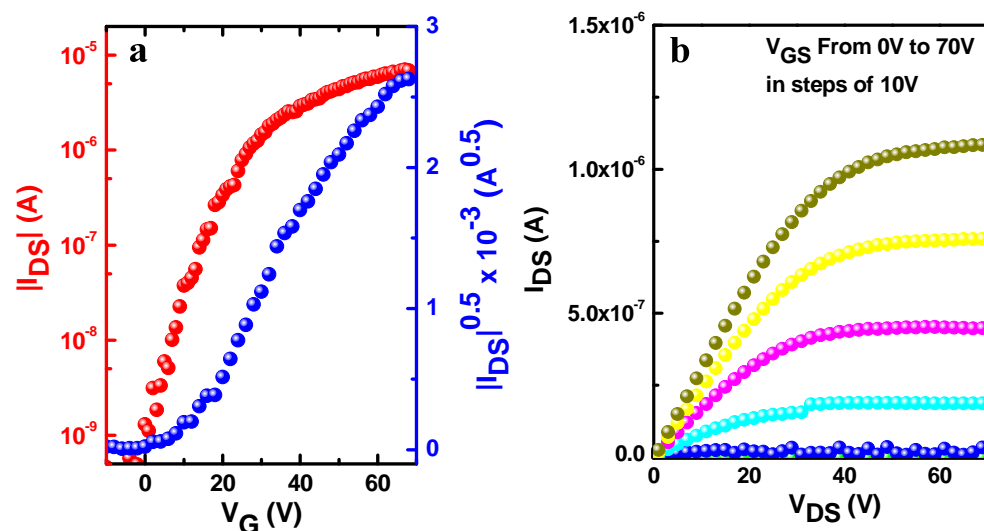


Figure S10. Transfer (a) and output (b) characteristic of the OFETs based on ODI-CN. The thin film was prepared from DCB solution on bare SiO_2/Si substrate followed by annealing 230°C . The devices were measured in nitrogen.

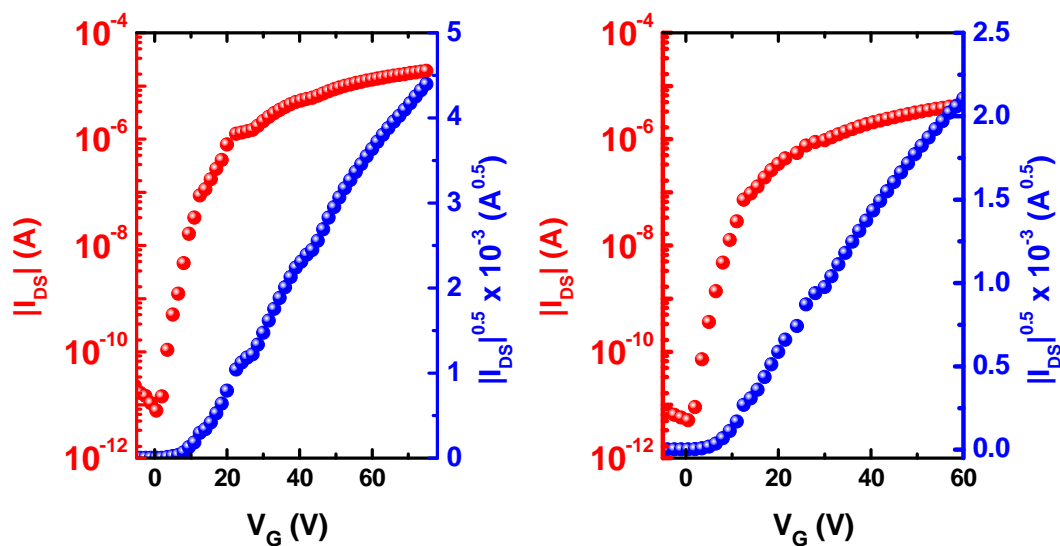


Figure S11. Transfer characteristic of the OFETs based on ODI-CN. The thin film was prepared from DCB (left) and CHCl_3 (right) solution on bare SiO_2/Si substrate followed by annealing $230\text{ }^\circ\text{C}$. The devices were measured in air.

9. AFM images of thin films of ODI-CN

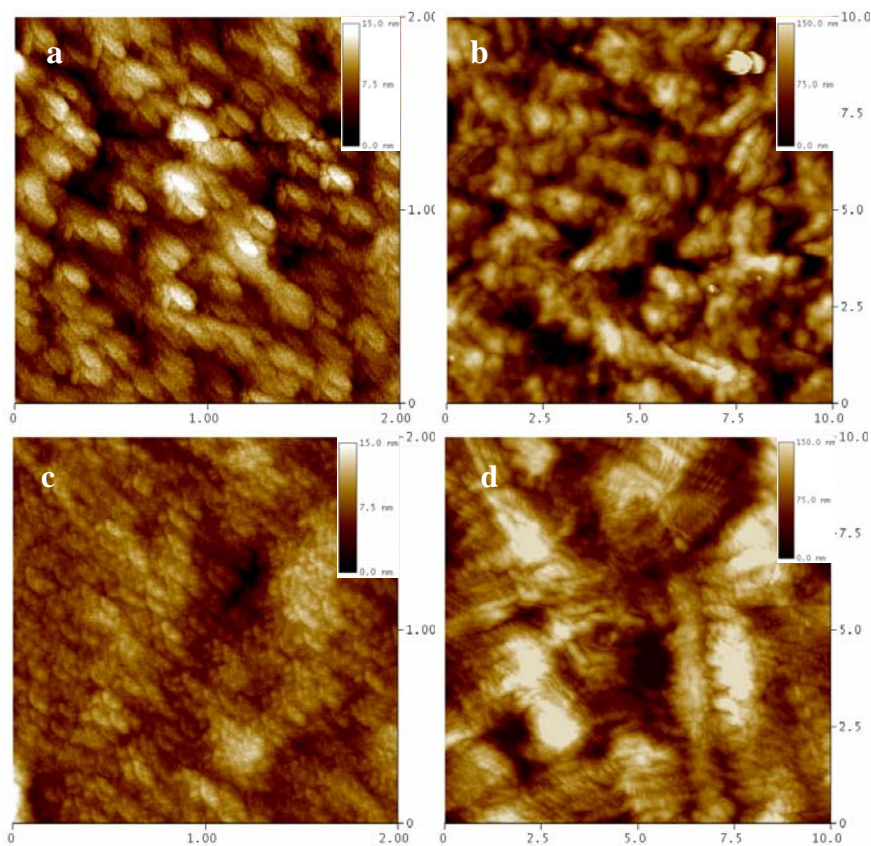


Figure S12. Tapping mode AFM images of the thin films of ODI-CN on bare SiO_2/Si substrate prepared by different methods. (a) annealed and (c) as spun film: spin-coated from chloroform solution; (b) annealed and (d) as cast film: drop-casted from DCB solution.

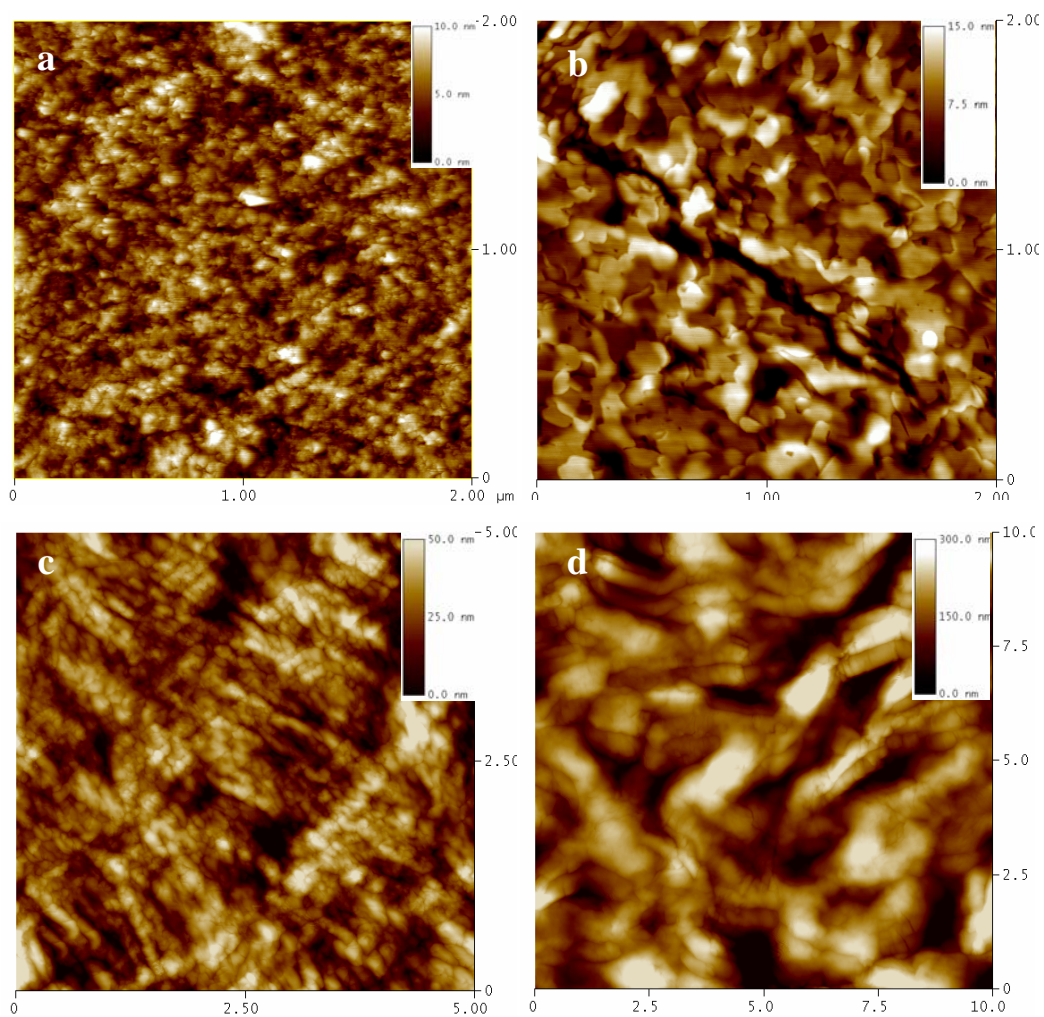


Figure S13. Tapping mode AFM images of the thin films of ODI-CN on OTCS treated SiO_2/Si substrate spin-coated from CHCl_3 solution: (a) as cast and (b) annealed film. drop-casted from DCB solution: (c) as cast and (d) annealed film.

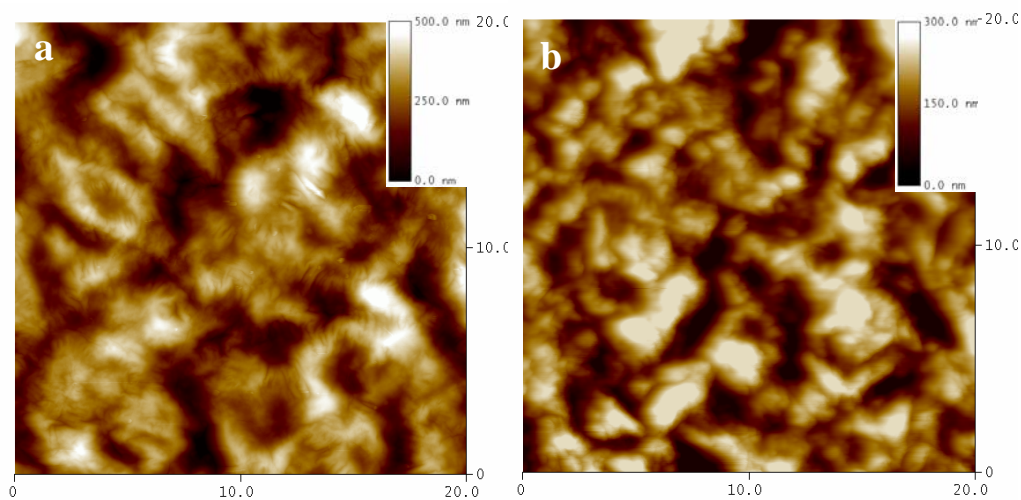


Figure S14. Tapping mode AFM images of the thin films of ODI-CN on OTMS treated SiO_2/Si substrate drop-casted from DCB solution: (a) as cast and (b) annealed film.

10. Thin film XRD patterns of ODI-CN

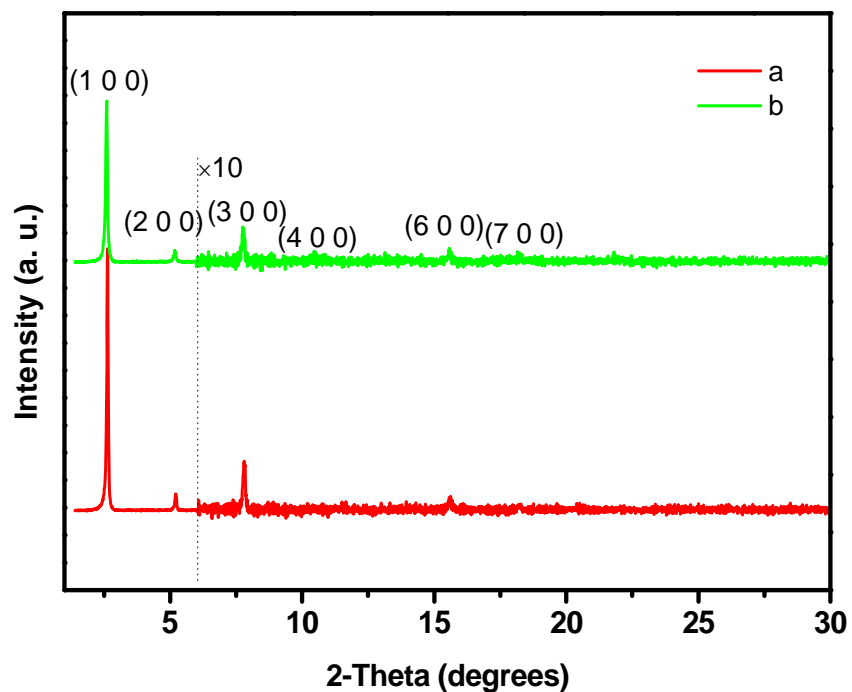


Figure S15. XRD pattern of ODI-CN thin film prepared by drop-coating from DCB solution followed by annealing at 230 °C: (a) pristine surface. (b) OTCS treated substrate.

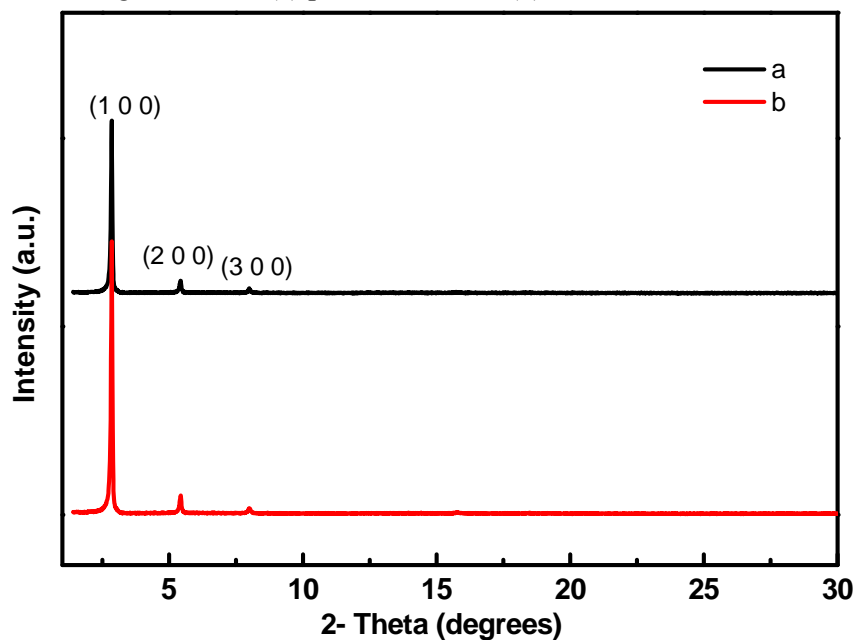


Figure S16. XRD pattern of ODI-CN thin film prepared by drop-coating from DCB solution onto OTMS treated substrate: (a) as cast, (b) annealed.

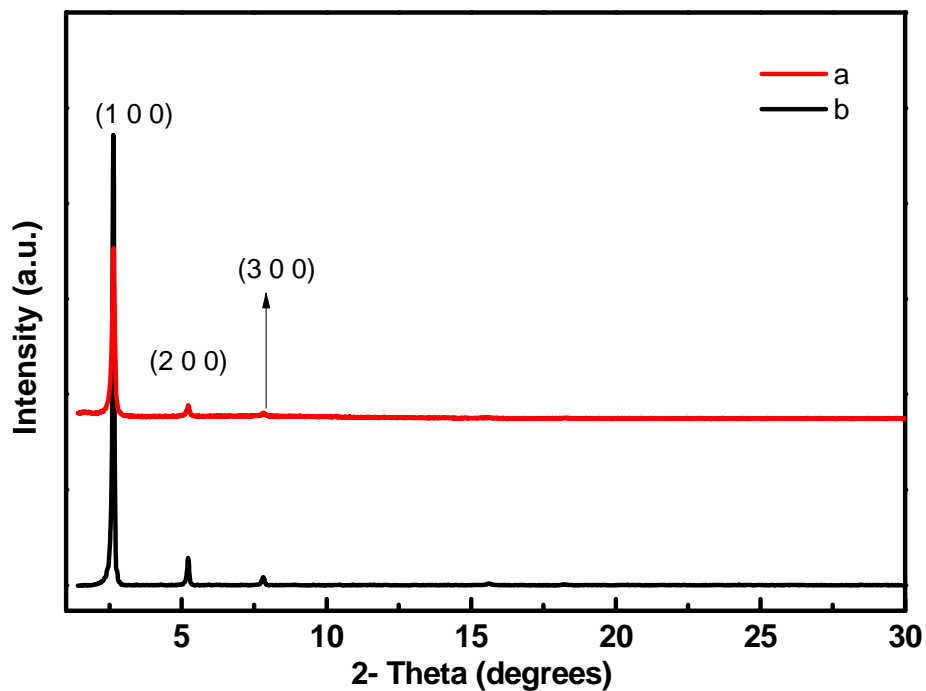


Figure S17. XRD pattern of ODI-CN thin film prepared by drop-coating from DCB solution onto OTCS treated substrate: (a) as cast, (b) annealed.

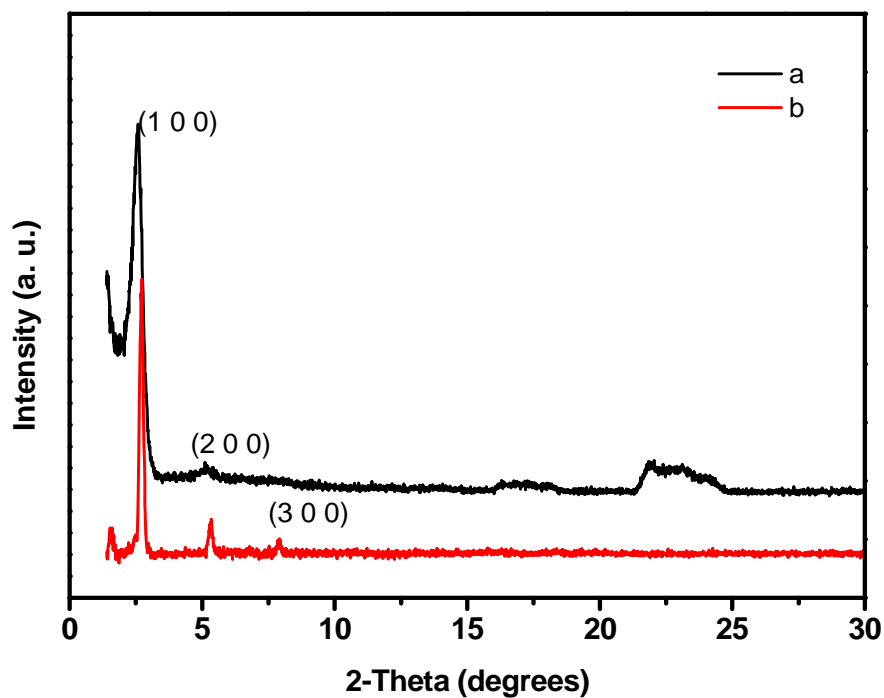


Figure S18. XRD pattern of ODI-CN thin film prepared by spin-coating from CHCl_3 solution onto OTCS treated substrate: (a) as spun, (b) annealed film.

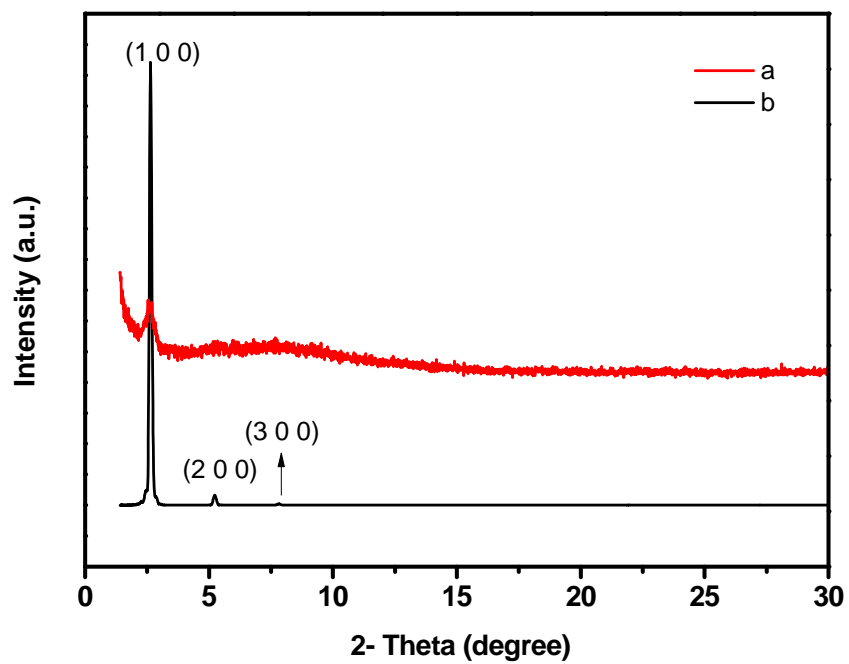
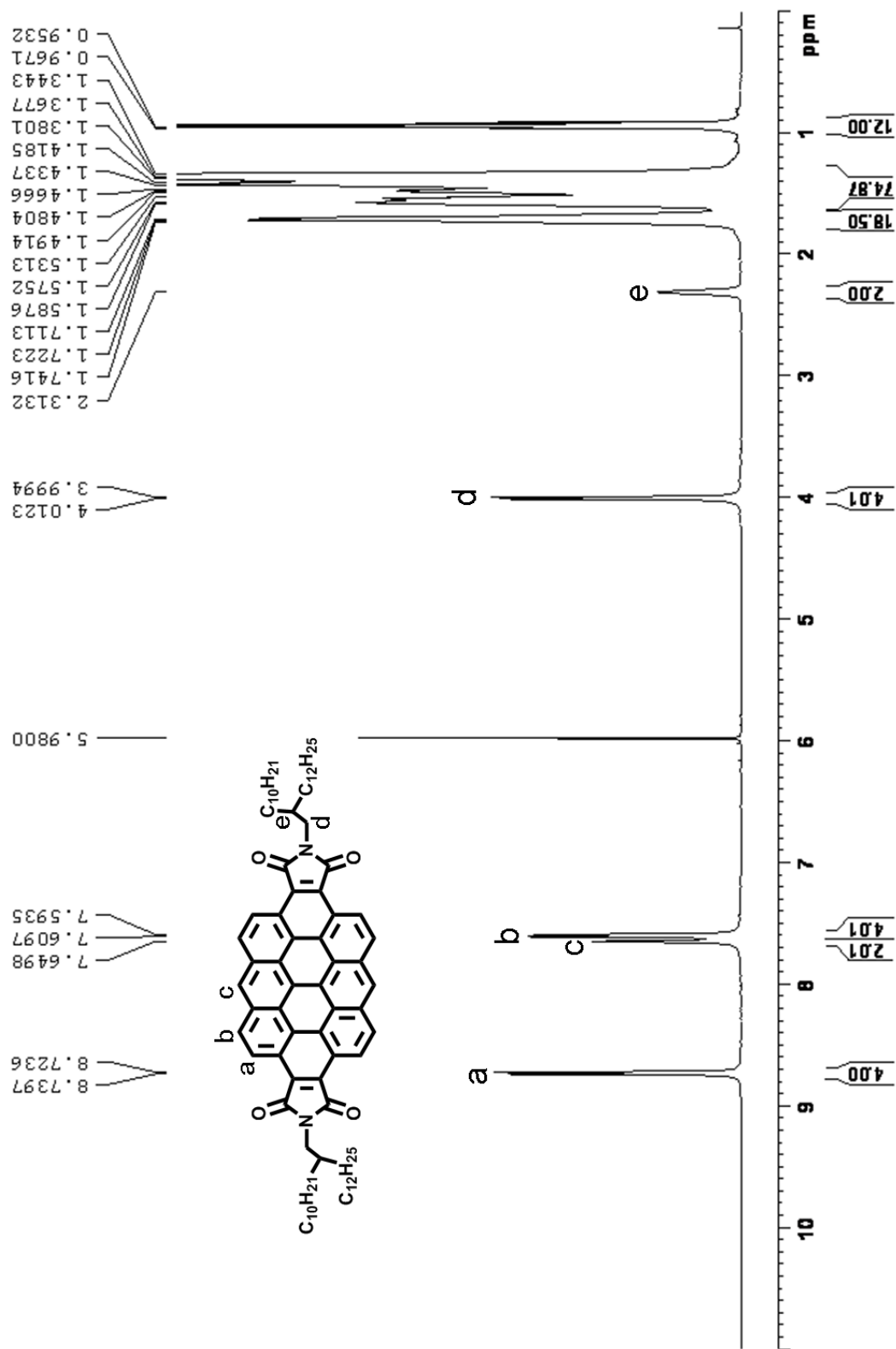
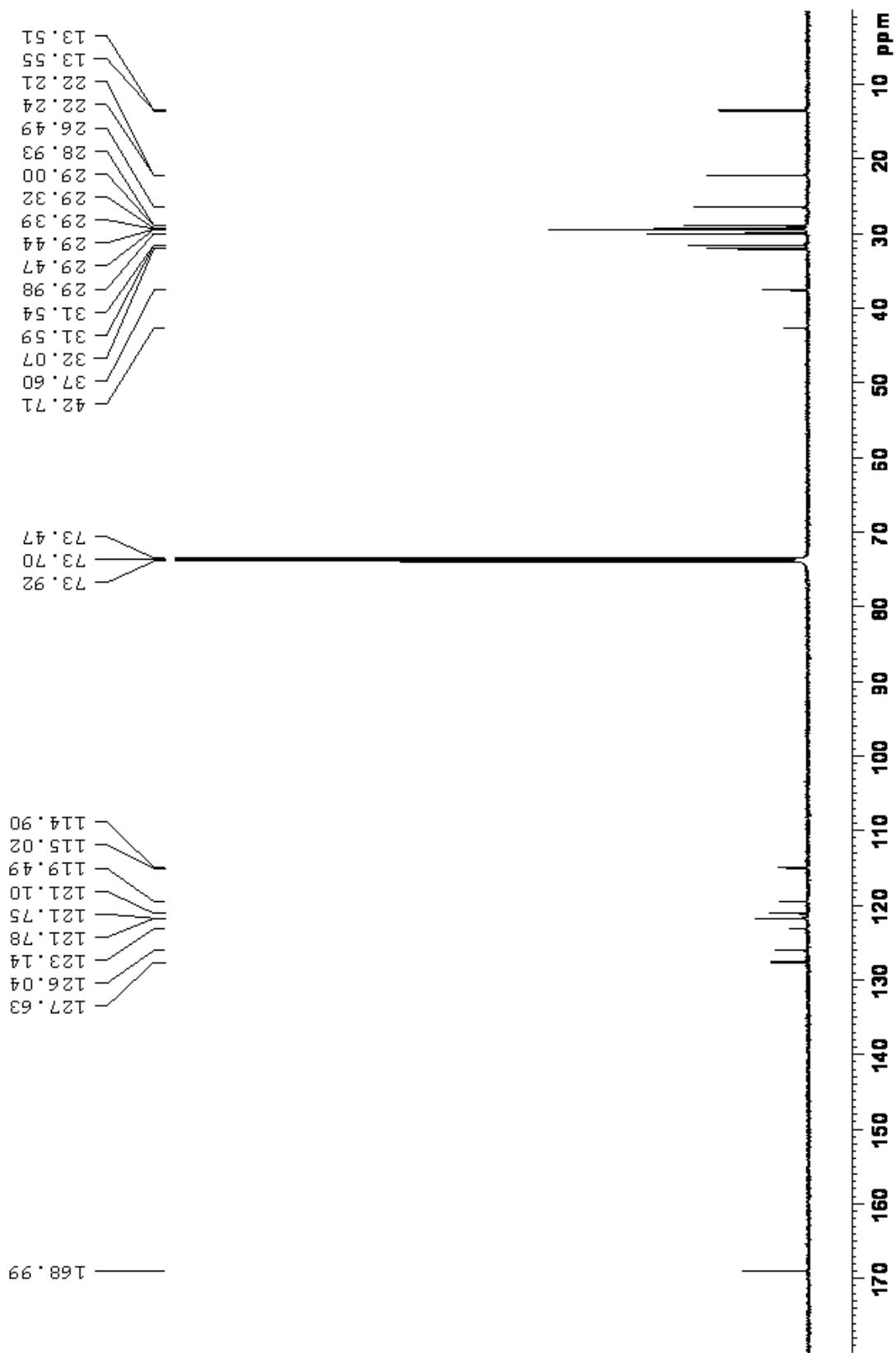
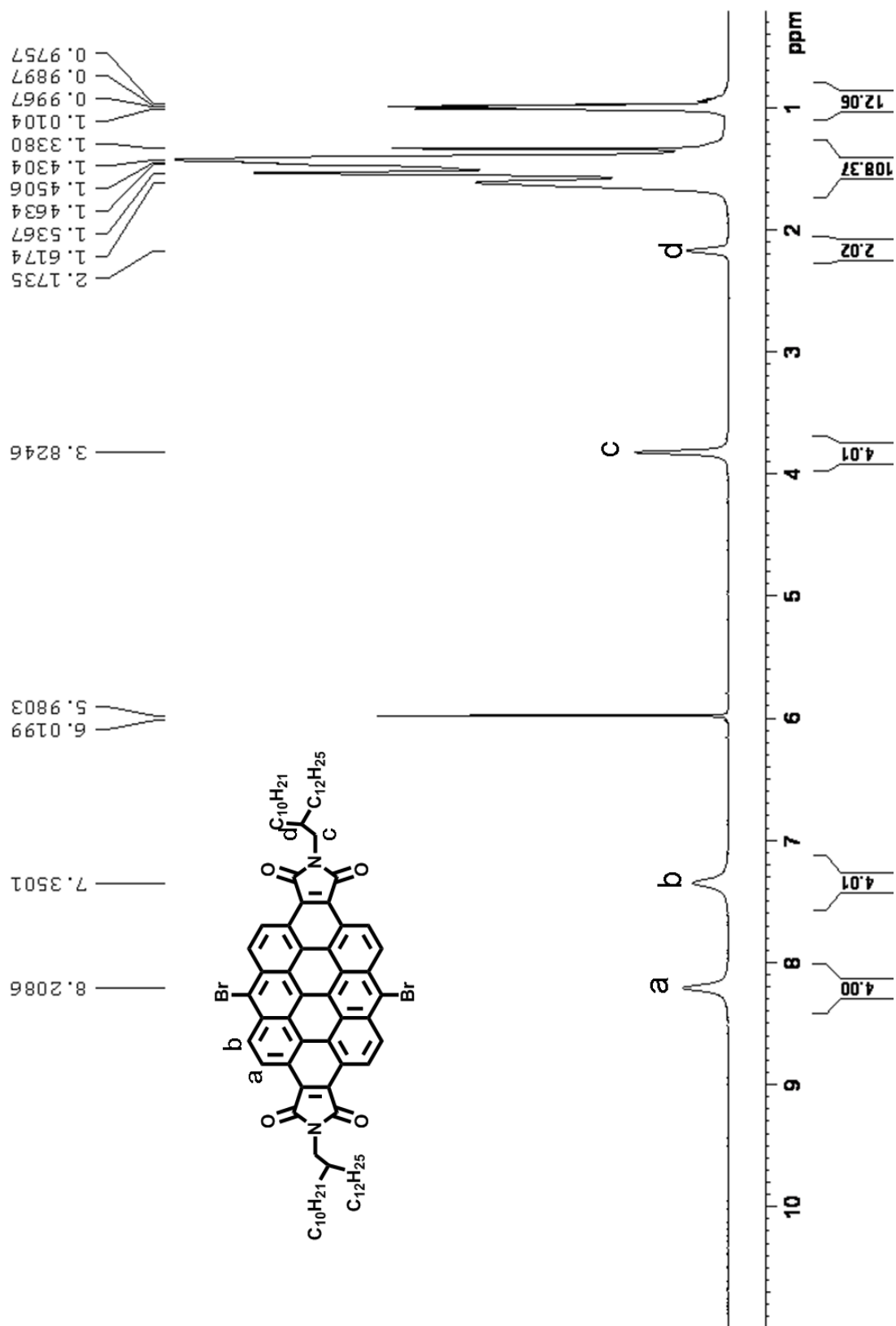


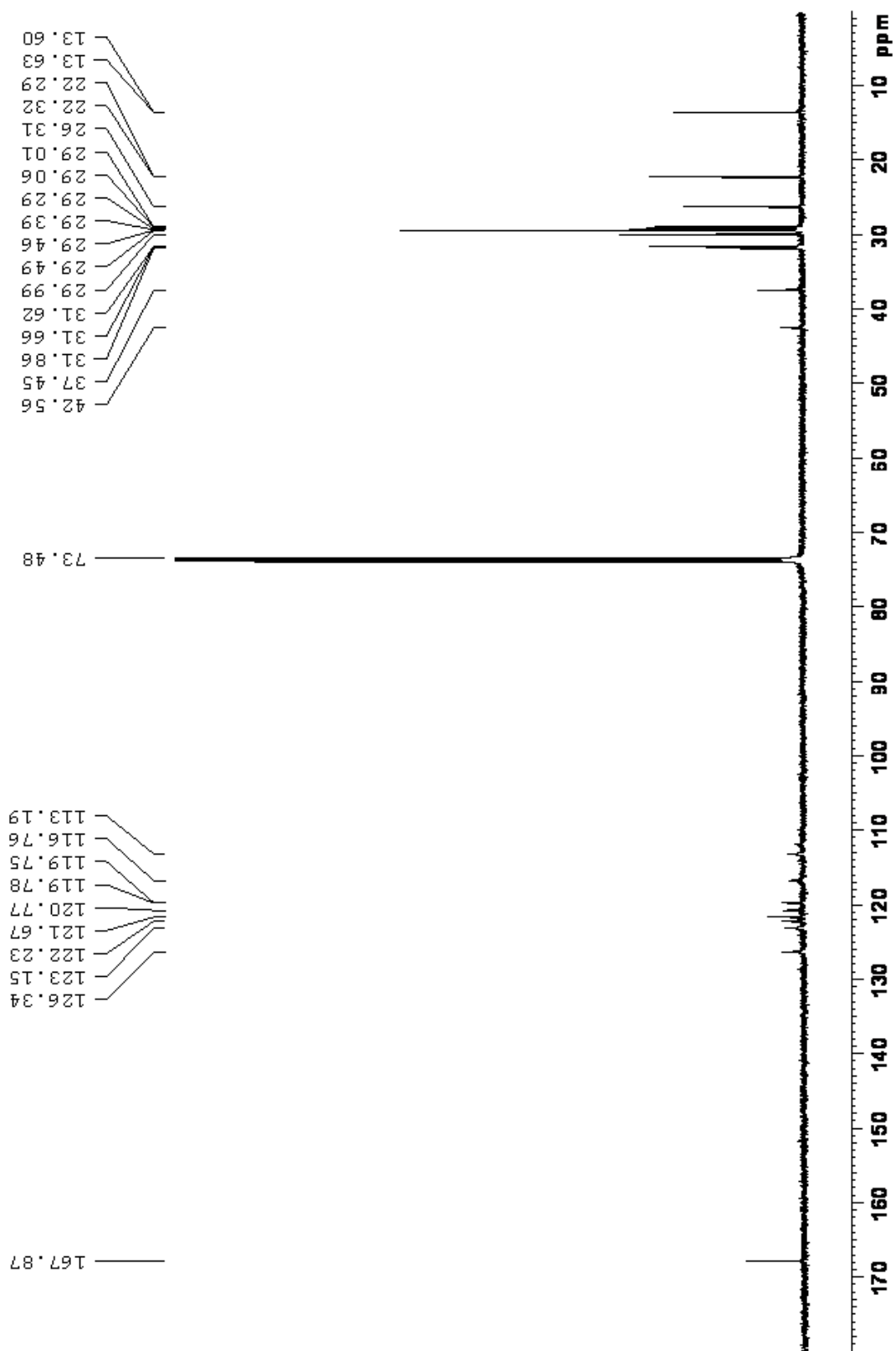
Figure S19. XRD pattern of ODI-CN thin film prepared by spin-coating from CHCl_3 solution onto bare substrate: (a) as spun, (b) annealed film.

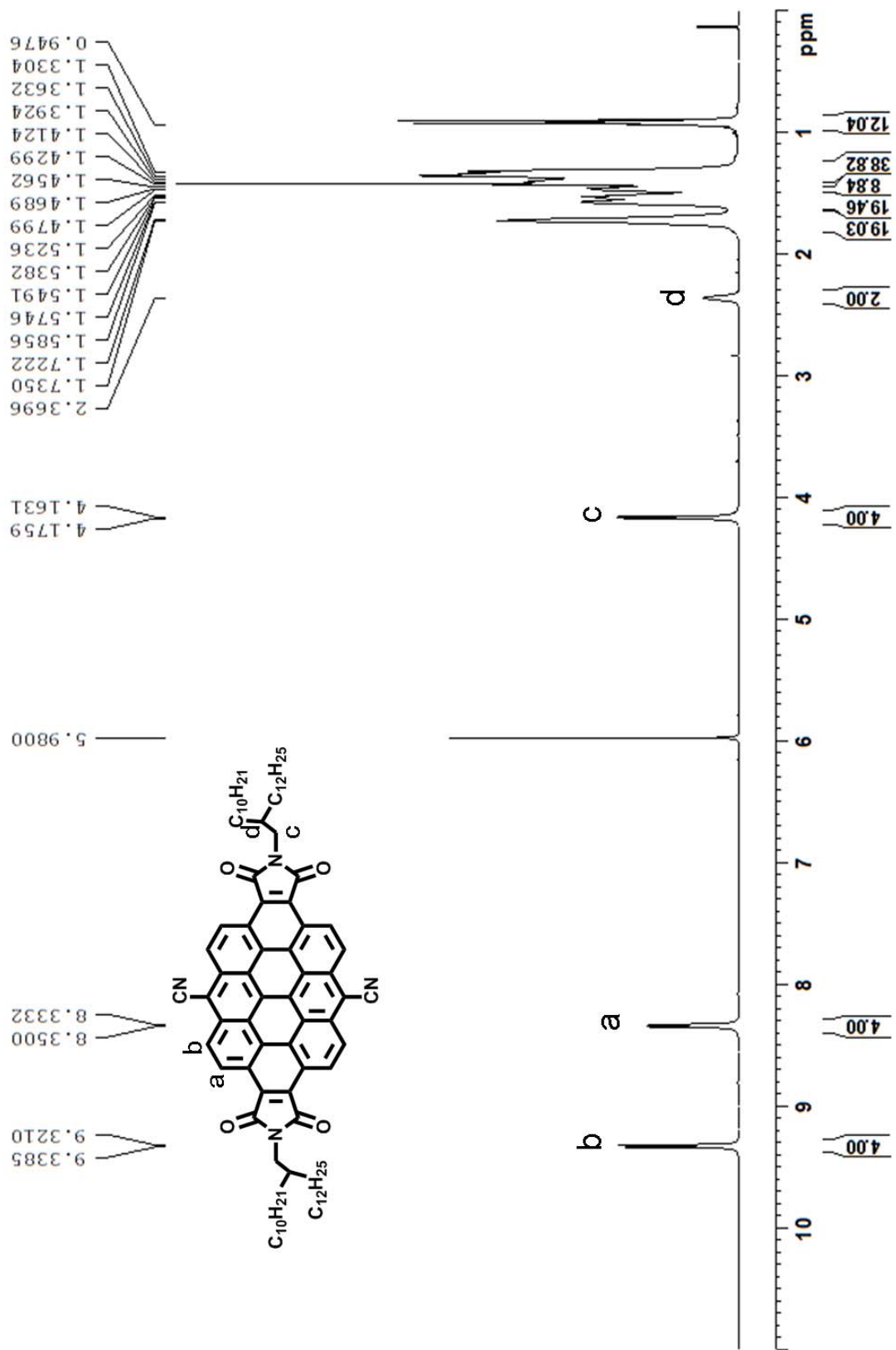
11. ^1H NMR (500 MHz), ^{13}C NMR (125 MHz) spectra of ODI, ODI-Br and ODI-CN recorded at 100 °C in $\text{CDCl}_2\text{CDCl}_2$.











12. MALDI-TOF mass spectra of ODI, ODI-Br and ODI-CN

